Implementation of subloading constitutive models in Material Point Methods

Carlos Pereira

Abstract

This document describes the work developed in the short term scientific mission, STSM, of the COST TU1202, entitled *Implementation of subloading constitutive models in material point methods*, hosted by Dr. Phil Vardon, in the Technical University of Delft, TU Delft. A dynamic version of the material point method, MPM, in two-dimension was programmed, with the computer language Fortran. An elastoplastic subloading soil model with anisotropy, cyclic behaviour and structure was implemented in the program. The constitutive model was integrated using an explicit algorithm.

1 Introduction

This document describes the work developed in the short term scientific mission, STSM, of the COST TU1202, entitled *Implementation of subloading constitutive models in material point methods*, hosted by Dr. Phil Vardon, in the Technical University of Delft, TU Delft.

According to the work plan summary submitted to the COST TU1202, the main objective of this STSM was to evaluate the possibility to implement an extension to unsaturated soils of a viscoplastic subloading soil model with anisotropy, cyclic behaviour and structure, developed by the STSM participant to saturated soils (Maranha et al., 2016), in the implicit material point method (Wang et al., 2016), IMPM, and then study the behaviour of the slopes due to suction changes.

The initial meeting, realised in the first day of the STSM, the way how both, the IMPM and the constitutive model, should interact were analysed. Due to the way how the IMPM was implemented and the complex task that an implicit integration of this type of constitutive model was, and taking into account the future perspective of the work initiated with this STSM, it was decided to make some changes to the initial work plan, reformulated to include the following main tasks:

- Implementation of a dynamic version of the material point method, MPM, in two-dimension. The computer language used to make this implementation was Fortran and all the programming structure was thought to be easy to interact with complex constitutive models and to expand to three-dimensional problems.

- Implementation of an elastoplastic subloading soil model with anisotropy, cyclic behaviour and structure in the MPM. The constitutive model was integrated using an explicit algorithm.

The implementation of the MPM was described in section 2. In the section 3 the constitutive model is briefly presented. In section 4 the results of a slope collapse is presented. Finally, the conclusions and some future actions between that had been planned during the STSM are presented in section 5.

2 Implementation of MPM

The material point method, MPM, which is considered a mesh-based particle method, can be conceived as an extension of the finite element method, FEM, in which soil and structural bodies are represented by Lagrangian particles that move through an Eulerian fixed mesh. The physical properties of the continuum, such as mass, momentum, material constants and state variables, strains, stresses as well as external loads, reside with material particles that are not fixed to a mesh, but move through the mesh allowing possibilities of modelling large deformations. The Eulerian mesh carries no permanent information, with the exception of some type of boundary conditions. Hence, MPM combines the best aspects of both Lagrangian and Eulerian formulations and avoids as much as possible the shortcomings of them.

Based on Chen and Brannon (2002) and Al-Kafaji (2013), a dynamic version of MPM was implemented. The computer language used to make this implementation was Fortran and all the programming structure was thought to be easy to interact with complex constitutive models and to expand to three-dimensional problems.

Compared with the based works, the MPM implemented does not restring the initial position of the material points to the Gauss points of the mesh. Instead, the material points are distributed before the mesh definition. This is an important contribution to have different densities of material points without the necessity to define complex mesh geometries.

Another improvement made is related with the algorithm that find in which element a material point method is located. In this version, when a material point changes from element, instead of the program locks for the material point in all the elements list, first it will lock in the surrounding elements. Taking into account that the time increment is always very small, this procedure is less time consuming.

Finally, the program was paralysed using the OpenMP to decrease the time needed to get a solution. However, during the STSM, there was no time to do a complete validation of the implementation.

An overview of the overall MPM solution procedure for a single time step is here given. Let us consider the state of a continuum at time t and briefly describe the procedure of advancing the solution to time $t + \mathrm{d}t$. For a complete description of the procedure, see Chen and Brannon (2002) and Al-Kafaji (2013). The solution procedure for a single time step consists of the following steps:

1. For each material point p that is located inside of the element e, the mapping operation from material points to local nodes i of the element e is performed for mass, $\boldsymbol{m}_e^t$, momentum, $\mathbf{p}_e^t$, gravity force, $\mathbf{F}_e^{t,\mathrm{grav}}$, and internal force, $\mathbf{F}_e^{t,\mathrm{int}}$, through the following equations

$$\boldsymbol{m}_e^t = m_{e,i}^t = \sum_{p=1}^{n_{ep}} m_p \, N_i\big(\boldsymbol{\xi}_p^t\big) \ , \tag{1}$$

$$\mathbf{p}_e^t = \boldsymbol{p}_{e,i}^t = \sum_{p=1}^{n_{ep}} m_p \boldsymbol{v}_p^t \, N_i\big(\boldsymbol{\xi}_p^t\big) \ , \tag{2}$$

$$\mathbf{F}_e^{t,\mathrm{grav}} = \boldsymbol{F}_{e,i}^{t,\mathrm{grav}} = \sum_{p=1}^{n_{ep}} m_p \, \boldsymbol{g} N_i\big(\boldsymbol{\xi}_p^t\big) \tag{3}$$

and

$$\mathbf{F}_e^{t,\mathrm{int}} = \boldsymbol{F}_{e,i}^{t,\mathrm{int}} = \sum_{p=1}^{n_{ep}} \boldsymbol{B}_i^T\big(\boldsymbol{\xi}_p^t\big) \, \boldsymbol{\sigma}_p^t \, \Omega_p^t \, , \tag{4}$$

where m_p is the mass of material point p, n_{ep} the number of material points inside the element e, N_i the shape function of the local node i, $\boldsymbol{\xi}_p^t$ the location of the material point

p in local coordinates at time t, $\boldsymbol{v}_p^t$ the velocity of the material point p at time t, $\boldsymbol{g}$ the vector of gravitational acceleration, $\boldsymbol{B}_i$ the gradient of the shape function of the local node i, $\boldsymbol{\sigma}_p^t$ the stress tensor of the material point p at time t and Ω_p^t the volume of the material point p at time t.

2. Assembly procedure from the local nodes i, $\boldsymbol{m}_e^t$, $\mathbf{p}_e^t$, $\mathbf{F}_e^{t,\text{grav}}$ and $\mathbf{F}_e^{t,\text{int}}$, to the mesh nodes n, $\boldsymbol{m}^t$, $\mathbf{p}^t$, $\mathbf{F}^{t,\text{grav}}$ and $\mathbf{F}^{t,\text{int}}$, respectively.

3. For each mesh node n, determine the nodal accelerations at time t, $\boldsymbol{a}_n^t$, according to

$$\boldsymbol{a}_n^t = \frac{\boldsymbol{F}_n^{t,\text{grav}} - \boldsymbol{F}_n^{t,\text{int}}}{m_n^t} \,. \tag{5}$$

4. The velocities of material points p ate time $t + \mathrm{d}t$ are updated from the mesh node accelerations

$$\boldsymbol{v}_p^{t+\mathrm{d}t} = \boldsymbol{v}_p^t + \sum_{i=1}^{n_{ln}} \boldsymbol{a}_i^t \, N_i\big(\boldsymbol{\xi}_p^t\big) \, \mathrm{d}t \tag{6}$$

where n_{ln} is the number of local nodes of the shape function. For each material point p it is necessarily to established a relationship between the local nodes numeration i and the mesh nodes n.

5. The nodal velocities $\boldsymbol{v}_n^{t+\mathrm{d}t}$ at time $t + \mathrm{d}t$ are calculated from the updated material point velocities $\boldsymbol{v}_p^{t+\mathrm{d}t}$, performing the mapping operations of the momentum at $t + \mathrm{d}t$ from material points p to local nodes of the element e where the material point p is located

$$\boldsymbol{p}_{e,i}^{t+\mathrm{d}t} = \sum_{p=1}^{n_{ep}} m_p \boldsymbol{v}_p^{t+\mathrm{d}t} \, N_i\big(\boldsymbol{\xi}_p^t\big) \;, \tag{7}$$

assemble the momentum from local nodes, $\boldsymbol{p}_{e,i}^{t+\mathrm{d}t}$, to mesh nodes, $\boldsymbol{p}_n^{t+\mathrm{d}t}$, and perform the following equation

$$\boldsymbol{v}_n^{t+\mathrm{d}t} = \frac{\boldsymbol{p}_n^{t+\mathrm{d}t}}{m_n^t} \tag{8}$$

6. The current velocity gradient of material point p at time $t + \mathrm{d}t$, $\mathbf{L}_p^{t+1}$, is given by

$$\mathbf{L}_p^{t+\mathrm{d}t} = \sum_{i=1}^{n_{ln}} \boldsymbol{v}_i^{t+\mathrm{d}t} \boldsymbol{B}_i\big(\boldsymbol{\xi}_p^t\big) \tag{9}$$

and which allows the determination of the strain increment, $\mathrm{d}\boldsymbol{\varepsilon}_p^{t+\mathrm{d}t}$, and spin increment, $\mathrm{d}\boldsymbol{\omega}_p^{t+\mathrm{d}t}$, of the material point p as

$$\mathrm{d}\boldsymbol{\varepsilon}_p^{t+\mathrm{d}t} = \frac{1}{2}\left[\mathbf{L}_p^{t+\mathrm{d}t} + \big(\mathbf{L}_p^{t+\mathrm{d}t}\big)^T\right] \mathrm{d}t \tag{10}$$

and

$$\mathrm{d}\boldsymbol{\omega}_p^{t+\mathrm{d}t} = \frac{1}{2}\left[\mathbf{L}_p^{t+\mathrm{d}t} - \big(\mathbf{L}_p^{t+\mathrm{d}t}\big)^T\right] \mathrm{d}t \tag{11}$$

7. Find the stress increment, $\mathrm{d}\boldsymbol{\sigma}$, and tensorial and scalar state variables of constitutive model, $\mathrm{d}\mathbf{h}$ and $\mathrm{d}h$, respectively, from the constitutive model for the given strain increment. To take into account the effect of rotation, it is necessarily to correct stress tensor and tensorial state variables of the spin effect, according to

$$\boldsymbol{\sigma}_p^t = \boldsymbol{\sigma}_p^t + \mathrm{d}\boldsymbol{\omega}_p^{t+\mathrm{d}t}\boldsymbol{\sigma}_p^t - \boldsymbol{\sigma}_p^t \, \mathrm{d}\boldsymbol{\omega}_p^{t+\mathrm{d}t} \tag{12}$$

and

$$\mathbf{h}_p^t = \mathbf{h}_p^t + \mathrm{d}\boldsymbol{\omega}_p^{t+\mathrm{d}t}\mathbf{h}_p^t - \mathbf{h}_p^t\,\mathrm{d}\boldsymbol{\omega}_p^{t+\mathrm{d}t} \tag{13}$$

and update the particle stress tensor and state variables.

8. Volume, $\Omega_p^{t+\mathrm{d}t}$, and mass density, $\rho_p^{t+\mathrm{d}t}$, of the material point p at time $t+\mathrm{d}t$ are updated using the volumetric strain increment, $\mathrm{d}\varepsilon_{\mathrm{v,p}}^{t+\mathrm{d}t} = \operatorname{tr}\boldsymbol{\varepsilon}_p^{t+\mathrm{d}t}$, as

$$\Omega_p^{t+\mathrm{d}t} = \left(1 + \mathrm{d}\varepsilon_{\mathrm{v,p}}^{t+\mathrm{d}t}\right)\Omega_p^t \tag{14}$$

and

$$\rho_p^{t+\mathrm{d}t} = \frac{\rho_p^t}{\left(1 + \mathrm{d}\varepsilon_{\mathrm{v,p}}^{t+\mathrm{d}t}\right)} \tag{15}$$

9. Mesh nodal velocities are integrated to get mesh nodal incremental displacements $\mathrm{d}\boldsymbol{u}_n^{t+\mathrm{d}t}$ and coordinates $\mathrm{d}\boldsymbol{x}_n^{t+\mathrm{d}t}$, as

$$\mathrm{d}\boldsymbol{u}_n^{t+\mathrm{d}t} = \mathrm{d}t\,\boldsymbol{v}_n^{t+\mathrm{d}t} \tag{16}$$

and

$$\mathrm{d}\boldsymbol{x}_n^{t+\mathrm{d}t} = \mathrm{d}\boldsymbol{x}_n^t + \mathrm{d}\boldsymbol{u}_n^{t+\mathrm{d}t} \tag{17}$$

10. Displacements, $\boldsymbol{u}_p^{t+\Delta t}$, and position of material points, $\boldsymbol{x}_p^{t+\Delta t}$, are updated from the mesh nodes

$$\boldsymbol{u}_p^{t+\mathrm{d}t} = \boldsymbol{u}_p^t + \sum_{i=1}^{n_{ln}} \mathrm{d}\boldsymbol{u}_i^{t+\mathrm{d}t} N_i\left(\boldsymbol{\xi}_p^t\right) \tag{18}$$

and

$$\boldsymbol{x}_p^{t+\mathrm{d}t} = \boldsymbol{x}_p^t + \sum_{i=1}^{n_{ln}} \mathrm{d}\boldsymbol{x}_i^{t+\mathrm{d}t} N_i\left(\boldsymbol{\xi}_p^t\right)\ . \tag{19}$$

11. Find the new elements for those particles that have left the old elements. Consequently, the new number of particles per each finite element must be determined and the active and inactive elements must be identified. The new local position, $\boldsymbol{\xi}_p^{t+\mathrm{d}t}$, of each particle inside the element must be obtained.

3 Constitutive model

As mentioned in section 1, it was implemented in MPM an elastoplastic subloading soil model with anisotropy, cyclic behaviour and structure in the MPM. The constitutive model was integrated using an explicit algorithm. In this report, a briefly presentation of the model is presented because the complete presentation of the model is part of a paper that will be submitted to a journal during March.

The model is based on the subloading surface concept that enables the occurrence of elastoplastic strains inside the yield surface. The subloading surface is defined geometrically simply as being homothetic to the yield surface relative to a given centre of homothety, located inside the yield surface, implying the definition of a homothety ratio or scaling factor.

Fig. 1 schematically represents, in the effective stress space, $\boldsymbol{\sigma}$, the homothetic surfaces that define the elastoplastic subloading model with a mobile centre of homothety, $\mathbf{a}$, where $p = 1/3\operatorname{tr}\boldsymbol{\sigma}$ is the mean stress, $\mathbf{s} = \operatorname{dev}\boldsymbol{\sigma}$ the deviatoric stress and $\mathbf{I}$ the second order identity tensor. Considering that $\boldsymbol{\sigma}_{\mathrm{y}} = \mathbf{a} + 1/R\,(\boldsymbol{\sigma} - \mathbf{a})$ is the homothetic image of $\boldsymbol{\sigma}$ on the yield surface relative to $\mathbf{a}$, respectively, R is the homothety ratio of the subloading surface relative to the yield surface, respectively.

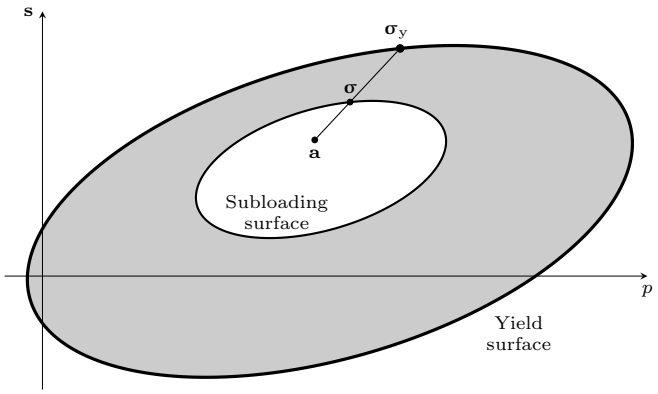

Figure 1: Schematic representation, in $\boldsymbol{\sigma}$ space, of the homothetic surfaces that define the elastoplastic subloading model with a mobile centre of homothety, $\mathbf{a}$.

3.1 Yield and subloading surfaces

$\overline{f}$ and f designate the subloading and yield functions, respectively, where the subloading surface is a surface in stress space homothetic to the yield surface relative to point $\mathbf{a}$ with scaling factor R. The subloading surface can be determined from the yield surface as

$$\overline{f}\left(\boldsymbol{\sigma}\right) = f\left(\boldsymbol{\sigma}_{\mathrm{y}}\right)\big|_{\boldsymbol{\sigma}_{\mathrm{y}}=\mathbf{a}+\frac{1}{R}(\boldsymbol{\sigma}-\mathbf{a})} = 0\,. \tag{20}$$

Using the Modified Cam Clay Model yield surface as the foundation of the model, the yield surface is given by

$$f\left(\boldsymbol{\sigma}\right) = \left(\frac{\overline{q}}{M}\right)^2 + \overline{p}\left(\overline{p} - p_{\mathrm{c}}\right) = 0 \tag{21}$$

with

$$\overline{p} = p + \xi p_{\mathrm{c}}\,, \tag{22}$$

$$\overline{q} = \sqrt{\frac{3}{2}}\left\|\overline{\mathbf{s}}\right\| \tag{23}$$

and

$$\overline{\mathbf{s}} = \mathbf{s} - p\boldsymbol{\beta}\,, \tag{24}$$

where $\boldsymbol{\beta}$ is a second order non-dimensional deviatoric tensor that describes anisotropy, ξ a model constant used to allow some isotropic tensile strength, p_{c} the size of the structured (bonded) yield surface along the hydrostatic axis and M a constant defining the eccentricity of the yield surface.

3.2 Elastic law

In order to represent the elastic behaviour, a hypoelastic model was adopted. The increment of the effective stress tensor, $\mathrm{d}\boldsymbol{\sigma}$, is defined by

$$\mathrm{d}\boldsymbol{\sigma} = K\,\mathrm{d}\varepsilon_{\mathrm{v}}^{\mathrm{e}}\mathbf{I} + 2G\,\mathrm{d}\mathbf{e}^{\mathrm{e}} \tag{25}$$

with

$$K = \frac{p + p_{\mathrm{e}}}{\overline{\kappa}} \tag{26}$$

and

$$G = \frac{3\left(1-2\nu\right)}{2\left(1+\nu\right)}K\,, \tag{27}$$

where K and G are the variable bulk and shear moduli, respectively, $\mathrm{d}\varepsilon_{\mathrm{v}}^{\mathrm{e}} = \mathrm{tr}\,\mathrm{d}\boldsymbol{\varepsilon}^{\mathrm{e}}$ the increment of the elastic volumetric strain, $\mathrm{d}\mathbf{e}^{\mathrm{e}} = \mathrm{dev}\,\mathrm{d}\boldsymbol{\varepsilon}^{\mathrm{e}}$ the increment of the elastic deviatoric strain tensor, $\mathrm{d}\boldsymbol{\varepsilon}^{\mathrm{e}}$ the increment of the elastic strain tensor, p_{e} a material constant defined as the mean effective stress for which the specific volume v becomes infinite, i.e., $v \to +\infty$ when $p \to -p_{\mathrm{e}}$, $\overline{\kappa}$ the slope of the elastic isotropic compression line in $(\ln p, \ln v)$ representation plane and ν the constant Poisson's ratio.

3.3 Plastic strain increment

Assuming non-associated plastic flow, the increment of the plastic strain is defined as

$$\mathrm{d}\boldsymbol{\varepsilon}^{\mathrm{p}} = \begin{cases} 0 & \text{if} \quad R \leq R_{\min} \\ \mathrm{d}\Lambda \dfrac{\partial\, \overline{g}\,(\boldsymbol{\sigma})}{\partial \boldsymbol{\sigma}} & \text{if} \quad R > R_{\min} \end{cases}, \tag{28}$$

where $\overline{g}\,(\boldsymbol{\sigma})$ is the subloading plastic potential function, $\mathrm{d}\Lambda$ the plastic multiplier increment and $R_{\min}$ a small value to prevent the singularity that occurs when $\boldsymbol{\sigma} = \mathbf{a}$.

A homothetic relationship is assumed between the subloading plastic potential function and the plastic potential function with the same scaling factor as the subloading surface, R, such that

$$\overline{g}\,(\boldsymbol{\sigma}) = g\,(\boldsymbol{\sigma}_{\mathrm{y}})\big|_{\boldsymbol{\sigma}_{\mathrm{y}} = \mathbf{a} + \frac{1}{R}(\boldsymbol{\sigma} - \mathbf{a})} \tag{29}$$

with

$$g\,(\boldsymbol{\sigma}) = \left(\frac{\overline{q}}{\alpha M}\right)^2 + \overline{p}\,(\overline{p} - p_{\mathrm{c}})\ , \tag{30}$$

where α is the constant defining non-associativity (if $\alpha = 1$ the model is associated).

3.4 Hardening laws

3.4.1 Subloading hardening

The subloading hardening law, represented by the evolution of the subloading homothetic ratio R, is defined by

$$\mathrm{d}R = \begin{cases} \mathrm{d}R^{\mathrm{e}} & \text{if} \quad R \leq R_{\min} \\ -c_{\mathrm{R}} \ln\left(\dfrac{R - R_{\min}}{1 - R_{\min}}\right) \|\mathrm{d}\boldsymbol{\varepsilon}^{\mathrm{p}}\| & \text{otherwise} \end{cases} \tag{31}$$

where c_{R} is a model constant and $\mathrm{d}R^{\mathrm{e}}$ is the increment of R due to $\mathrm{d}\boldsymbol{\sigma}^{\mathrm{e}} = \mathcal{D} : \mathrm{d}\boldsymbol{\varepsilon}$ in a strain controlled process and simply due to $\mathrm{d}\boldsymbol{\sigma}$ in a stress controlled process. $\mathcal{D} = K\mathbf{I} \otimes \mathbf{I} + 2G\,(\mathcal{I} - 1/3\mathbf{I} \otimes \mathbf{I})$ is the fourth order tensor of elastic tangent moduli.

3.4.2 Anisotropic hardening

The anisotropy tensor hardening law was defined such that $\boldsymbol{\beta}$ moves towards the deviatoric stress tensor, $\mathbf{s}$. It is assumed that, if the stress follows a radial deviatoric path, passing through the hydrostatic axis, the anisotropy tensor will tend to align itself with $\mathbf{s}$. The critical state condition, defined by the stress ratio at failure, M_{cs}, defines an isotropic surface because it is assumed that, at the critical state, the initial soil anisotropy has already been erased and $\boldsymbol{\beta}$ is aligned with $\mathbf{s}$ (at least along radial deviatoric stress paths). Therefore, an anisotropic hardening limit surface, $\eta_{\beta,\mathrm{cs}}$, is defined.

The anisotropic hardening law is defined by

$$\mathrm{d}\boldsymbol{\beta} = c_{\beta}\, \|\mathrm{d}\mathbf{e}^{\mathrm{p}}\|\, \frac{p}{p_{\mathrm{atm}}} \left(\sqrt{\frac{2}{3}}\eta_{\beta,\mathrm{cs}}\,(\theta_{\overline{\mathbf{s}}})\, \frac{\overline{\mathbf{s}}}{\|\overline{\mathbf{s}}\|} - \boldsymbol{\beta}\right), \tag{32}$$

where c_β is a material model constant, p_{atm} the atmospheric pressure and $\mathrm{d}\mathbf{e}^{\text{p}} = \operatorname{dev}\mathrm{d}\boldsymbol{\varepsilon}^{\text{p}}$ the increment of the plastic deviatoric strain tensor. The critical state surface is defined as $M_{\text{cs}}(\theta_{\overline{\mathbf{s}}}) = M_{\text{c}}\, h(\theta_{\overline{\mathbf{s}}})$, where $h(\theta_{\overline{\mathbf{s}}})$ is obtained according to Willam and Warnke (1975).

3.4.3 Isotropic hardening

The isotropic hardening incorporates the evolution of the soil's structure (debonding) and is controlled by the internal variable p_{c} that defines the size of the yield surface. p_{c}, defined as

$$p_{\text{c}} = R_{\text{b}}\,\overline{p}_{\text{c}}\,, \tag{33}$$

has two components: the mean yield stress for the unbonded material, $\overline{p}_{\text{c}}$, and the bonding factor, R_{b}. Therefore, its rate is given by

$$\mathrm{d}p_{\text{c}} = R_{\text{b}}\,\mathrm{d}\overline{p}_{\text{c}} + \overline{p}_{\text{c}}\,\mathrm{d}R_{\text{b}}\,. \tag{34}$$

The isotropic hardening of the unbonded material, $\mathrm{d}\overline{p}_{\text{c}}$, is a function of the plastic volumetric strain increment, $\mathrm{d}\varepsilon_{\text{v}}^{\text{p}} = \operatorname{tr}\mathrm{d}\boldsymbol{\varepsilon}^{\text{p}}$, as

$$\mathrm{d}\overline{p}_{\text{c}} = \left(\overline{p}_{\text{c}} + \frac{p_{\text{e}}}{1-\xi}\right)\frac{\mathrm{d}\varepsilon_{\text{v}}^{\text{p}}}{\overline{\lambda}-\overline{\kappa}} \tag{35}$$

where $\overline{\lambda}$ is the slope of the normal compression line in $(\ln p, \ln v)$ representation space.

The evolution of bonding factor, $\mathrm{d}R_{\text{b}}$, is given by

$$\mathrm{d}R_{\text{b}} = c_{\text{b}}\,(R_{\text{bf}} - R_{\text{b}})\,\|\mathrm{d}\boldsymbol{\varepsilon}^{\text{p}}\| \tag{36}$$

where c_{b} is a material constant specifying the rate of debonding and $R_{\text{bf}} \geq 1$ the unbonding limit for large strains, that assumes the value 1 if total debonding is considered achievable. As a result,

$$\mathrm{d}p_{\text{c}} = \frac{R_{\text{b}}}{\overline{\lambda}-\overline{\kappa}}\left(\frac{p_{\text{c}}}{R_{\text{b}}} + \frac{p_{\text{e}}}{1-\xi}\right)\mathrm{d}\varepsilon_{\text{v}}^{\text{p}} + \frac{p_{\text{c}}}{R_{\text{b}}}c_{\text{b}}\,(R_{\text{bf}} - R_{\text{b}})\,\|\mathrm{d}\boldsymbol{\varepsilon}^{\text{p}}\|\,. \tag{37}$$

3.4.4 Centre of homothety hardening

The movement of the centre of homothety is given by

$$\mathrm{d}\mathbf{a} = c_{\text{a}}\,\|\mathrm{d}\boldsymbol{\varepsilon}^{\text{p}}\|\,(\overline{\boldsymbol{\sigma}}_{\text{y}} - \mathbf{a}) + \frac{\mathrm{d}p_{\text{c}}}{p_{\text{c}}}\mathbf{a} + p_{\text{a}}\,\mathrm{d}\boldsymbol{\beta} \tag{38}$$

where $p_{\text{a}} = 1/3\operatorname{tr}\mathbf{a}$ and c_{a} is a material constant that determines how fast $\mathbf{a}$ moves towards the point $\overline{\boldsymbol{\sigma}}_{\text{y}}$. This hardening law has the following two important aspects:

1. To assure that, during isotropic and anisotropic hardening of the yield surface, the centre of homothety stays inside the yield surface.

2. The movement of $\mathbf{a}$ is directed towards $\overline{\boldsymbol{\sigma}}_{\text{y}} = \mathbf{c} + (1-\delta)\,(\boldsymbol{\sigma}_{\text{y}} - \mathbf{c})$, which is the homothetic image of $\boldsymbol{\sigma}_{\text{y}}$ on a surface that is slightly smaller than the yield surface, controlled by the constant δ, with the centre of homothety coinciding with the centre of yield surface, $\mathbf{c}$. This aspect is introduced to avoid the point ever being on the yield surface, which may cause numerical stability problems.

3.5 Model constants and initial values of internal variables.

In its most general form, this model has 14 constants and 4 initial values of internal variables. Some of the constants can be obtained directly from laboratory tests. $\overline{\kappa}$ and $\overline{\lambda}$ can be determined from an isotropic compression test with unloading. ν and M_{c} can be determined from drained or undrained triaxial compression tests and k from drained or undrained triaxial extension tests. In the absence of triaxial extension results, the value of k could be assumed to be the same as the Mohr-Coulomb model one, which gives $k = 3/(3 + M_{\mathrm{c}})$. The other constants and variables interact in a complex way and may need an optimisation algorithm to enable their determination. Presently, this issue may not necessarily be a problem due to the development of heuristic general optimisation techniques such as the genetic algorithm Pereira et al. (2014).

R_{min} and δ are not model constants as they do not influence the model's response. They assume small values in order to avoid numerical problems and singularities and do not need to be determined from laboratory tests. For unstructured soils, ξ and p_{e} assume small values to allow for a small tensile strength value and avoid zero or negative elastic moduli, respectively.

Since the model is modular in its formulation, when certain aspects of soil behaviour are not relevant, it can assume simpler forms that do not need all of the constants and variables to be determined. For instance, the traditional elastoplastic response (elastic behaviour inside of the yield surface) is reproduced by assuming a large value for c_{R}. When cyclic loading is not important $\mathbf{a} = \mathbf{0}$ and $c_{\mathrm{a}} = 0$. An associated flow rule requires $\alpha = 1$. An unstructured material is simulated with $R_{\mathrm{b}} = R_{\mathrm{bf}} = 1$ and $c_{\mathrm{b}} = 0$. The model becomes isotropic if $\boldsymbol{\beta} = \mathbf{0}$, $c_{\beta} = 0$ and $M = M_{\mathrm{c}}$. Finally, the model can even be reduced to the Modified Cam Clay model by assuming a large value for c_{R}, $\mathbf{a} = \mathbf{0}$, $c_{\mathrm{a}} = 0$, $\alpha = 1$, $R_{\mathrm{b}} = R_{\mathrm{bf}} = 1$, $c_{\mathrm{b}} = 0$, $\boldsymbol{\beta} = \mathbf{0}$, $c_{\beta} = 0$, $M = M_{\mathrm{c}}$, $k = 1$, $p_{\mathrm{e}} = 0$ and $\xi = 0$.

4 Results

In this section an example of a slope failure simulation, using the program developed during the STSM, is presented. Figure 2a represents the initial slope geometry and material points positions. At this stage, the slope is stable.

As represented in Figure 2b, a cut in the slope base was made. As a consequence of that, the slope started to move. Figures 2c–2e represent several configuration of the failure process.

5 Conclusions and future developments

The work developed in the short term scientific mission, STSM, of the COST TU1202, entitled *Implementation of subloading constitutive models in material point methods*, was presented.

As briefly described in section 2, a dynamic version of the material point method, MPM, in two-dimension was programmed, with the computer language Fortran. All the programming structure was thought to be easy to interact with complex constitutive models and to expand to three-dimensional problems. An elastoplastic subloading soil model with anisotropy, cyclic behaviour and structure was implemented in the program (see section 3). The constitutive model was integrated using an explicit algorithm.

As show in section 4, where an example of a slope failure is presented using all the tools developed during the STSM, the MPM is suitable to study problem with large strains (failure situation).

Concerning future developments and taking into account that this STSM was only the first stage of future collaborations into unsaturated soil behaviour and slope failure, with current projects which run for 3 or 4 years. In the next stage (during the current year) a conference

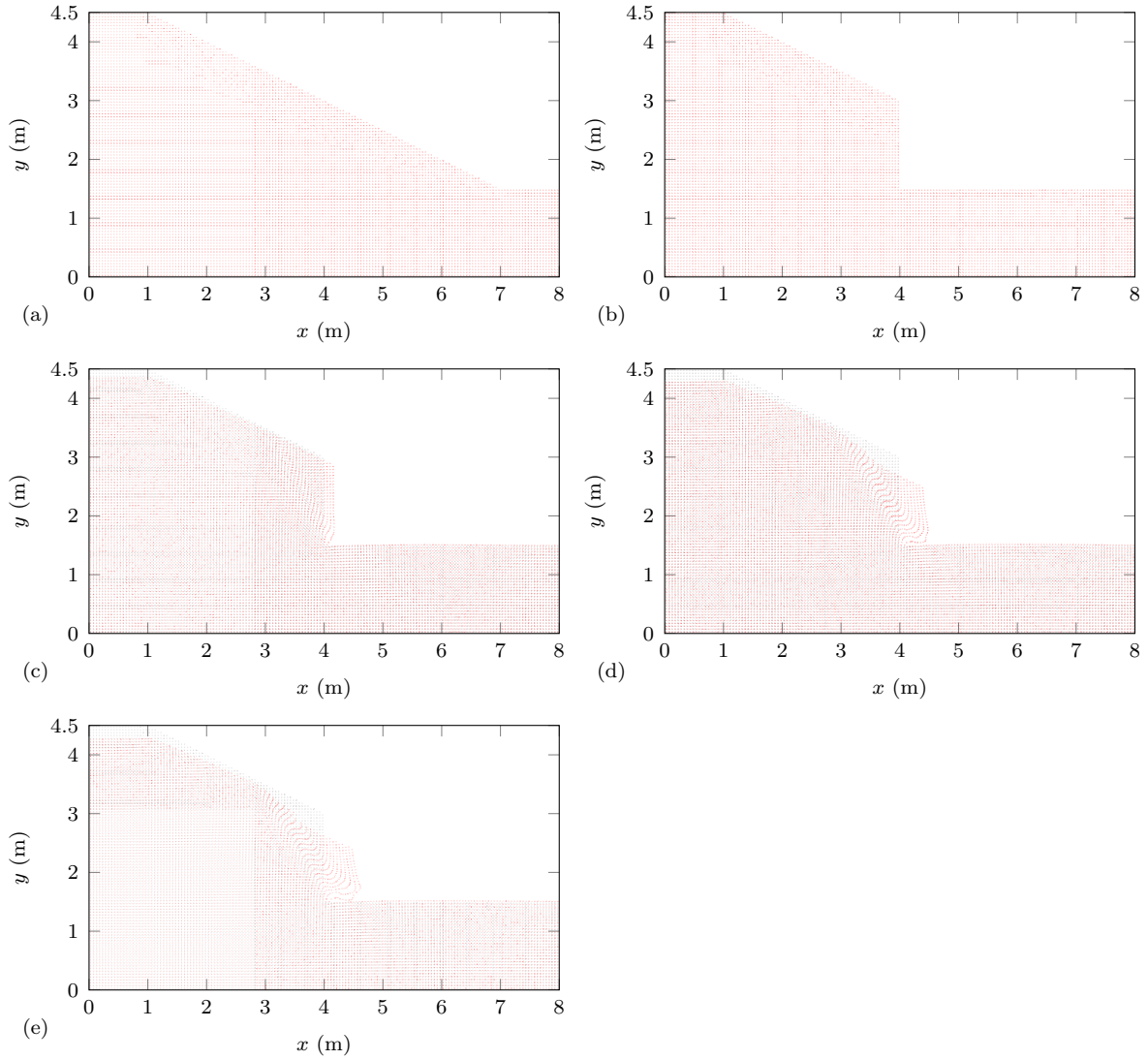

Figure 2: Geometrical position of the material points: (a) initial slope configuration, (b) geometry of the cut of the slope base, (c), (d) and (e) several position of the slope instability.

paper is going to be prepared where a numerical study of the influence of the several parameters of the constitutive model in the slope failure behaviour will be studied.

References

Al-Kafaji, I. K. J., 2013. Formulation of a dynamic material point method (MPM) for geomechanical problems. Ph.D. thesis, Institut für Geotechnik der Universität Stuttgart.

Chen, Z., Brannon, R., 2002. An evaluation of the material point method. Tech. rep., Sandia National Laboratories.

Maranha, J. R., Pereira, C., Vieira, A., 2016. A viscoplastic subloading soil model for rate dependent cyclic anisotropic structured behaviour. International Journal for Numerical and Analytical Methods in Geomechanics.

Pereira, C., Maranha, J. R., Brito, A., 2014. Advanced constitutive model calibration using genetic algorithms: some aspects. In: Hicks, M. A., Brinkgreve, R. B. J., Rohe, A. (Eds.),

Proc. 8th European Conference on Numerical Methods in Geotechnical Engineering, 18-20 June 2014, Delft, The Netherlands. CRC Press, Boca Raton, pp. 485–490.

Wang, B., Vardon, P. J., Hicks, M. A., Chen, Z., 2016. Development of an implicit material point method for geotechnical applications. Computers and Geotechnics 71, 159–167.

Willam, K. J., Warnke, E. P., 1975. Constitutive model for the triaxial behaviour of concrete. In: IABSE Seminar on Concrete Structures Subjected to Triaxial Stress. Vol. 19. Bergamo, Italy, pp. 1–30.